ELSEVIER

Deep-Sea Research II 53 (2006) 1144–1160

DEEP-SEA RESEARCH
PART II

www.elsevier.com/locate/dsr2

Distribution and circulation of water masses in the Gulf of Cadiz from in situ observations

Francisco Criado-Aldeanueva[a,*], Jesús García-Lafuente[a], Juan Miguel Vargas[a], Jorge Del Río[a], A. Vázquez[b], A. Reul[c], A. Sánchez[a]

[a]*Departamento de Física Aplicada II, Universidad de Málaga, Málaga, Spain*
[b]*Departamento de Física Aplicada, Universidad de Cádiz, Cádiz, Spain*
[c]*Departamento de Ecología y Geología, Universidad de Málaga, Málaga, Spain*

Received 1 February 2005; accepted 4 April 2006

Abstract

From data collected during GOLFO 2001 survey, a study was conducted on the circulation and distribution of water masses in the Gulf of Cadiz in the spring of 2001. The general surface circulation in the Gulf of Cadiz is anticyclonic with short-term, meteorologically induced variations. North Atlantic Central Water (NACW) ($\gamma_t = 26.6-27.3\,\mathrm{kg\,m^{-3}}$) is a representative water mass of the upper 1000 m of the water column. To the north, the lower part of the NACW layer ($\gamma_t = 27.3\,\mathrm{kg\,m^{-3}}$) is entrained by Mediterranean Water (MW) towards the open ocean while the upper layer ($\gamma_t = 26.6\,\mathrm{kg\,m^{-3}}$) forms part of the anticyclonic surface circulation of the Gulf of Cadiz. NACW mainly upwells in the vicinity of Capes St. Vincent and St. Maria. The upwelling off Cape St. Vincent is an open-sea process linked to a positive wind curl over the area, whereas the upwelling off Cape St. Maria is a more likely coastal process with a short time response to changes in the wind regime. The waters upwelled off Cape St. Vincent move eastwards following the main current until reaching ~7.5 °W, where they form the filament of Cape St. Maria, whose core flows at about 40–50 m. Wind changes from westerlies to easterlies produce important temporal variability in some spatial features (the upwelling off Cape St. Maria, the surface signature of the Huelva Front or the region of warm coastal waters) in a relatively shallow layer. Below this surface layer, the hydrological characteristics are fairly independent of meteorological forcing.
© 2006 Elsevier Ltd. All rights reserved.

Keywords: Gulf of Cadiz; Water masses; Geostrophic circulation; Upwelling processes; Cape St. Maria filament; Wind-induced variability

1. Introduction

The Gulf of Cadiz is the sub-basin of the North Atlantic nearest to the Strait of Gibraltar. Its northern, eastern and southern boundaries are well-defined by the southwest coasts of the Iberian Peninsula and by the Strait of Gibraltar and the Atlantic coast of Morocco, respectively. The western limit can be defined by the 9 °W meridian. On the Iberian coast, the most relevant geographical features are Cape St. Maria, Cape St. Vincent, and Cape Trafalgar (Fig. 1). To the east of Cape St. Maria the continental shelf is very wide (some

*Corresponding author. Tel.: +34 952 132849; fax: +34 952 131450.
E-mail address: fcaldeanueva@ctima.uma.es (F. Criado-Aldeanueva).

0967-0645/$ - see front matter © 2006 Elsevier Ltd. All rights reserved.
doi:10.1016/j.dsr2.2006.04.012

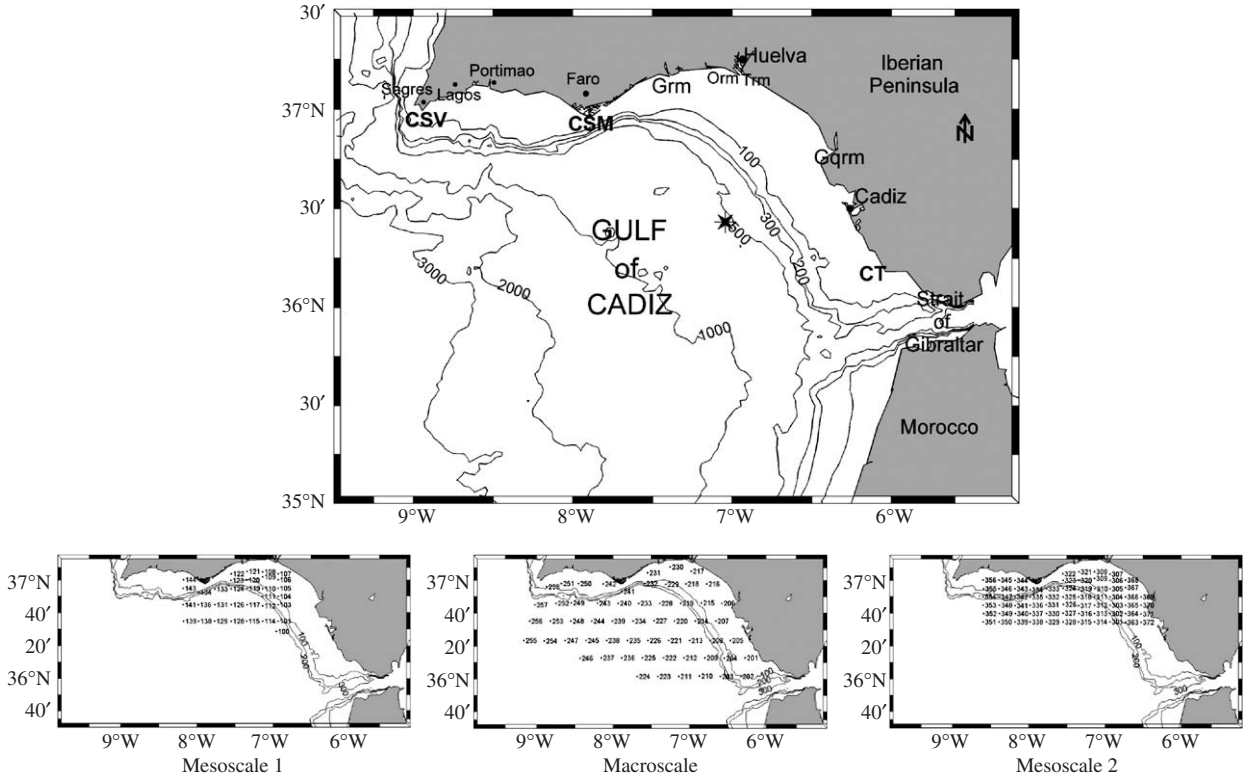

Fig. 1. Upper panel: Map of the Gulf of Cadiz showing the position of locations and other geographical features mentioned in the text. CT, CSM and CSV stand for Cape Trafalgar, Cape St. Maria and Cape St. Vincent, respectively. Grm, Orm, Trm and Gqrm stand for the mouths of Guadiana, Odiel, Tinto and Guadalquivir rivers, respectively. The star marks the position of the Red de Aguas Profundas (RAP) oceanographic buoy mentioned in the text. Lower panels show the station grid of the three legs (Mesoscale 1, Macroscale and Mesoscale 2) of GOLFO 2001 survey.

30–50 km) and has a gentle slope, whereas to the west it is narrow (<15 km) and its bottom is dotted with submarine canyons (Faro, Lagos, Portimao, St. Vincent, etc.).

The surface circulation of the Gulf of Cadiz, less studied than its deep circulation, is integrated into the general circulation of the Northeast Atlantic: the Azores current, which transports some 15 Sv between latitudes 35°N and 40°N to feed the Canary Current, frequently forms meanders that separate themselves from the main flow (Alves et al., 2002). Thus, the surface circulation of the Gulf of Cadiz could be understood as the last meander of the said Azores current. Part of this meander enters the Mediterranean Sea through the Strait of Gibraltar to balance evaporation and buoyancy losses within this Sea.

Stevenson (1977), combining in situ and sea-surface temperature (SST) satellite observations, identified an interesting thermal feature formed by a sequence of warm–cold–warm waters in NW–SE direction in the northeast part of the Gulf of Cadiz. Specifically, this feature is found between Cadiz and Huelva; Stevenson (1977) called it the 'Huelva Front'. Fiúza (1983), using wind data and SST images corresponding to the summer of 1979, correlated the occurrence of upwelling off the southwest coast of Iberia (and the appearance of the Huelva Front) with westerlies and the development of a warm coastal countercurrent stretching east–west with easterlies (Fiúza et al., 1982; Fiúza, 1983).

Folkard et al. (1997) analysed infrared SST satellite images throughout the year between July 1989 and March 1990 to provide a description of seasonal circulation patterns. An interesting outcome is the identification, at least in the summer months, of a bimodal pattern in SST images related to the wind regime. One of the patterns (related to westerlies) is characterised by an extension to the east of the upwelling off Cape St. Vincent, along with a signature of cold waters in the SE direction

from Cape St. Maria to the Strait of Gibraltar. The other configuration (related to easterlies) restricts the upwelling off Cape St. Vincent to a smaller area while, at the same time, the continental shelf of the southwest coast of Spain is flooded with warm waters and a new region of cold waters appears to the southwest of the Strait of Gibraltar.

More recently, Relvas and Barton (2002) have used a combined set of satellite data (1200 images between 1981 and 1995), coastal meteorological (wind, atmospheric pressure) and sea-level observations at strategic points to study different areas of interest: the upwelling off the western Portuguese coast, the upwelling off the south coast of the Iberian peninsula (Gulf of Cadiz), the filament off Cape St. Vincent, and the warm coastal countercurrent, all of them in relation to meteorological patterns. Sánchez and Relvas (2003) have analysed databases of hydrographic stations containing data for the entire 20th century (1900–1998) corresponding to spring and summer on the southwest coast of the Iberian Peninsula. Their analysis makes it possible, among other things, to identify the climatic patterns of circulation in the Gulf of Cadiz during the spring and summer months. The Portuguese Current flows southwards parallel to the western coast of the Iberian Peninsula and, when reaching Cape St. Vincent, it moves mainly towards the East. Once in the Gulf of Cadiz, the circulation is predominantly anticyclonic with some mesoscale meanders. Off Cape St. Maria, the main current turns to the south and then to the north and continues flowing parallel to the Spanish coast. Finally, the branch that separates from the Strait of Gibraltar forms an anticyclonic meander in the easternmost region which finally meets the Canary Current further southwest.

Vargas et al. (2003) have studied the evolution of thermal features in the Gulf of Cadiz using weekly SST images between 1993 and 1999 by means of spatial empirical orthogonal functions (EOF). The SST's first empirical mode (60% of variance) shows a clear north–south temperature gradient in the basin. The most outstanding characteristic is the nearly circular shape of (above average) warm waters in the southern part of the region under study. Likewise, this mode describes the upwelling area off Cape St. Vincent. The second empirical mode (13% of variance) shows a strong temporal variability and is chiefly responsible for the cooling and warming of the waters of the southwest Iberian continental shelf. Finally, the third mode (6% of variance) is well-correlated with the wind regime and allows to identify the areas of upwelling induced by this agent: one region off Capes St. Maria and St. Vincent, favoured by westerlies, and another located at the southwest extreme of the Strait of Gibraltar, favoured by easterlies.

Sub-surface in situ temperature observations collected during historical surveys (Rubín et al., 1999; Prieto et al., 1999; García et al., 2002) correlate reasonably well with satellite surface patterns and indicate a certain variability. In the survey of 1995, the tongue of cold water constituting the Huelva Front weakens and warm waters are seen to flood the shelf from the east of Cape St. Maria to the Guadalquivir river mouth, this being more pronounced between the latter and Cadiz. This description of the Huelva Front is compatible with an anticyclonic circulation. In addition, the estimate of geostrophic velocities confirms the hypothesis of anticyclonic circulation (García et al., 2002). In previous surveys (Rubín et al., 1997, 1999) this anticyclonic circulation is not evident on the surface, but it is in the sub-surface layer, thus supporting the hypothesis that this type of circulation is dominant, at least during summertime.

New data sets and results concerning this relatively poorly known area are presented in this paper, which is organised as follows: Section 2 presents the data and outlines the data processing and methodology. In Section 3, the spatial distribution and circulation of water masses, their large scale patterns and meteorologically forced variability are presented and discussed. Finally, Section 4 summarises the conclusions.

2. Data and methods

2.1. Data acquisition

The interdisciplinary survey GOLFO 2001 was carried out in the Gulf of Cadiz between 14 May and 3 June 2001 onboard the oceanographic research vessel Hespérides, within the framework of the project MAR99-0643, 'Distribution and Dynamics of Plankton and Seston in the Gulf of Cadiz: Variability Scales and Control by Physical and Biological Processes'. The survey was divided into three legs, called Mesoscale 1, Macroscale and Mesoscale 2, whose characteristics and geographical scope are shown in Table 1 and Fig. 1.

The data set includes hydrological data (Conductivity-Temperature-Depth, CTD Idronaut MK

Table 1
Characteristics of the three legs of the GOLFO 2001 survey

	Mesoscale 1	Macroscale	Mesoscale 2
Sample dates	14/05/01–16/05/01	17/05/01–24/05/01	29/05/01–02/06/01
No. of transects	7	12	11
Longitude range	6.92–8.18°W	6.27–9.28°W	6.51–8.59°W
Latitude range	36.58–37.08°N	36.01–37.13°N	36.57°N–37.08°N
Inclination	—	15°	—
Origin coordinates	8.3°W–36.54°N	(9.2°W–36.0°N)	(8.7°W–36.54°N)
Number of points	12×15	22×31	12×23

Inclination refers to the angle of deviation from the meridians. The last two rows are related to the optimal interpolation technique parameters (see Section 2.2).

137 with nephelometer and fluorometer SeaPoint and thermosalinographer SEABIRD SBE 21 for continuous recording of surface data), Acoustic Doppler Current Profiler (ADCP) velocity data (not used in this work), biological data (Rosette General Oceanics 1015 of 24 bottles), meteorological data (wind measurements taken with a scatterometer Quickscat, by the R/V Hespérides meteorological station and by the Red de Aguas Profundas (RAP network Puertos del Estado, see http://www.puertos.es) buoy of the Gulf of Cadiz), and satellite data (from National Oceanic and Atmospheric Administration, NOAA series). Some small gaps in the CTD and thermosalinographer data have been interpolated linearly. Larger gaps in the fluorometer data have been obviated.

2.2. Data processing: optimal interpolation

Following UNESCO (1985) the quantities γ_t and γ_θ, obtained from the temperature, salinity and pressure fields through the state equation are used to express the density field. The interpolation of the hydrological data was carried out by means of the optimal or statistical interpolation technique (OI henceforth). This method, widely presented in the literature (Gandin, 1963; Thiébaux and Pedder, 1987; Ruiz Valero, 2000; Gomis et al., 2001), is based on the condition that the differences between real field values and the results of the analysis are minimised statistically. In this work, the OI package worked out and broadcasted by the UIB-IMEDEA (Special Action CICYT, REN2000-2599-E) has been used.

This OI package, which includes a previous smoothing stage, requires the adjustment of several parameters: for the tendency's *degree of the polynomial* a low value is recommended and $n = 2$ has been used. The *spatial scale correlation,* or slope of the Gaussian used to adjust the correlations obtained from the survey data, has been established as 20 km, an appropriate value when mesoscale features dominate the dynamics. The *noise-signal* ratio allows us to introduce an estimate of observational error of analysed data into the analysis. The cross-validation technique provides values in the order of 0.001 for CTD data and in the order of 0.01 for ADCP data. The *interpolated grid step* should be a compromise between a grid dense enough to solve the scales of the features captured by sampling and the fact that the observational error is amplified on making spatial derivatives on a very dense grid. The condition $(1/4)\overline{d_{ki}} < \Delta x < (1/2)\overline{d_{ki}}$, where $\overline{d_{ki}}$ is the average distance between sampling points, provides a reasonable value. For the sake of homogeneity, the same spatial step has been chosen for the three legs, 0.1° in coordinate x (longitude) and 0.0548° in coordinate y (latitude). The difference lies in the origin of the grid and, consequently, in the number of grid points. The values of these parameters for each leg are shown in Table 1.

2.3. Data processing: EOF analysis

EOF analysis was introduced in the Earth sciences by Obukhov (1947) and Lorenz (1956). There are many examples in the literature concerning EOF analysis, mainly related to SST images (Hernández-Guerra and Nykjaer, 1997; Parada and Cantón, 1998; Álvarez et al., 2000; Vargas et al., 2003). In this work, it will be applied to the profiles of hydrological variables distributed all along the sampling grid to study the filament of Cape St. Maria in Section 3.4.

Assume a set of profiles of a specific variable on a defined domain with a dimension identical to the

number of levels considered (this will depend on the depth range of study). Each one of these vectors can be decomposed as the sum of an average value and an anomaly, that is

$$\vec{\varphi}_i = \overline{\vec{\varphi}} + \vec{\varphi}'_i, \tag{1}$$

where the mean $\overline{\vec{\varphi}}$ is defined as

$$\overline{\vec{\varphi}} = \frac{1}{N}\sum_{k=1}^{N} \vec{\varphi}_k, \tag{2}$$

where N is the total number of profiles (stations) and $i = 1, 2, \ldots, N_1$ indicates level i (N_1 is the number of levels). The covariance matrix of anomaly vectors between the different profiles is given by

$$C = C_{mn} = \frac{1}{N}\sum_{i=1}^{N_1} \varphi'_i(m)\varphi'_i(n) \tag{3}$$

with m, n being any two profiles. C is diagonalised according to $|C - \lambda I| = 0$, with I the identity matrix and λ a vector with the eigenvalues of C, which are real and verify: $C\vec{M}_p = \lambda_p \vec{M}_p$, where $\vec{M}_p (p = 1, 2, \ldots, N)$ are the eigenvectors (which constitute an orthogonal base) associated with the eigenvalue λ_p. Once the eigenvectors or modes have been calculated, the information at any depth can be expressed as a linear combination of the vectors of this base:

$$\vec{\varphi}_i = \overline{\vec{\varphi}} + \sum_{p=1}^{N} a_{ip}\vec{M}_p, \tag{4}$$

where $\vec{M}_p$ is the eigenvector corresponding to mode p and a_{ip} is the amplitude of the mode at level (depth) i, defined by $a_{ip} = \vec{M}_p \cdot \vec{\varphi}'_i$.

In this formulation, the eigenvectors (modes) represent an 'average' horizontal situation for all the sampled stations in the range of depths in which the analysis has been performed, while the amplitude of the corresponding mode (which depends on the depth) represents the importance in depth of the horizontal features depicted by the mode. To facilitate interpretation, the amplitude coefficients have been normalised to unit variance for each mode, the units of the corresponding variable remaining in the spatial maps of each mode.

3. Results and discussion

3.1. Water masses in the Gulf of Cadiz

In this section, the water masses detected in the Gulf of Cadiz will be analysed. Strictly speaking, a water mass is defined by its temperature and salinity taken as conservative parameters only altered by mixing. Following this requirement, some of the water classes described below are not water masses in the strict sense, although, by extension, in some cases all of them will be referred as water masses in general. Fig. 2 shows the *TS* diagram for Macroscale leg, which is the leg of greatest interest to identify water masses, owing to their wider geographical extension. The different waters found in the samplings can be listed as follows (see also Fig. 2):

(i) *North Atlantic Central Water* (*NACW*)*:* The linear behaviour in the *TS* diagram, characteristic of NACW, is found between $11.0\,^{\circ}\mathrm{C} \leqslant T \leqslant 17.0\,^{\circ}\mathrm{C}$; $35.6 \leqslant S \leqslant 36.5$ (although its most superficial region will be called SAW henceforth). Below a certain depth (from a certain isopycne), the *TS* diagram diverges from its former linear behaviour due to mixing with the underlying, salty Mediterranean Water (MW). In general, NACW shows a linear behaviour in the *TS* diagram for values of $26.6\,\mathrm{kg\,m^{-3}} \leqslant \gamma_\theta \leqslant 27.3\,\mathrm{kg\,m^{-3}}$, in good agreement with the description of Knoll et al. (1999) and Ambar et al. (2002).

(ii) *Surface Atlantic Water* (*SAW*)*:* This water has its origin in shallow NACW that has been modified by air–sea interactions so, strictly speaking, SAW is not a water mass. In the Gulf of Cadiz, SAW can be characterised for practical purposes as a region of the *TS* diagram with temperatures above $16.0\,^{\circ}\mathrm{C}$, $S \approx 36.4$ and $\gamma_t \leqslant 26.7\,\mathrm{kg\,m^{-3}}$, which is found between the surface and a depth of approximately 100 m over the entire region except for the continental shelf.

(iii) *Warm Shelf Waters* (*SW*)*:* At some of the sampled stations, mainly over the continental shelf, water warmer and fresher than SAW has been detected at the surface. This water comes from SAW that has been noticeably influenced by continental shelf processes, including heating and fresh water inputs from land. It corresponds to the points of the *TS* diagram between temperatures $14.0\,^{\circ}\mathrm{C} \leqslant T \leqslant 18.0\,^{\circ}\mathrm{C}$ (in Mesoscale 2 (not shown), the temperature is higher) and salinities $35.9 \leqslant S \leqslant 36.5$ that are placed outside the line of NACW. They

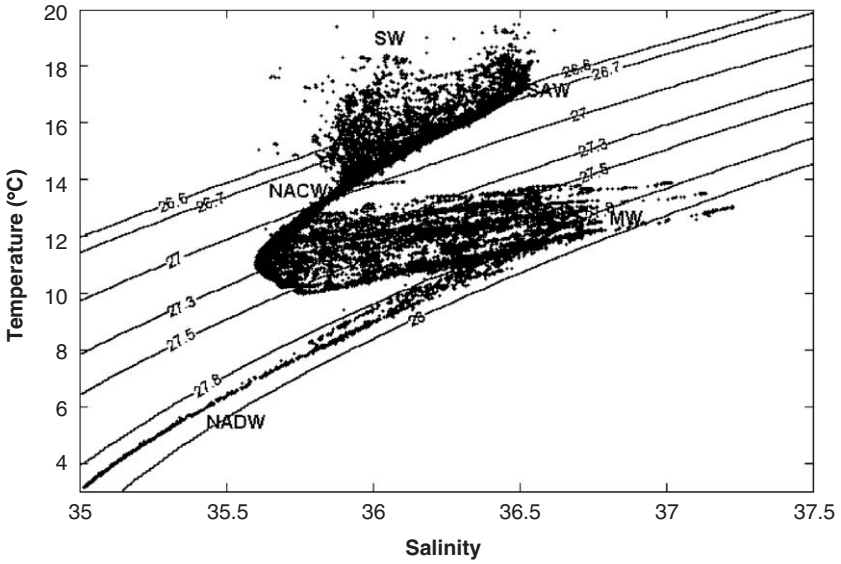

Fig. 2. Temperature–Salinity (*TS*) diagram of all the stations of the Macroscale leg during GOLFO 2001 survey. NACW, SAW, SW, MW and NADW are the acronyms for North Atlantic Central Water, Surface Atlantic Water, Shelf Water, Mediterranean Water and North Atlantic Deep Water, respectively. The labels are roughly located at the theoretical positions of these water masses on the *TS* diagram.

have been called Shelf Waters (SW) for practical purposes, although they are not a water mass in the strict sense.

(iv) *Mediterranean Water* (*MW*)*:* The analysis of the thermohaline properties of MW shows two main maxima in the *TS* diagram corresponding to two cores (upper and lower) with different densities, respectively, $\gamma_t \approx 27.5$ and $27.8\,\mathrm{kg\,m^{-3}}$ centred near 800 and 1200 m, in good agreement with number references from previous surveys (Madelain, 1970; Zenk, 1970; Ambar and Howe, 1979a, b; Ambar et al., 2002).

(v) *North Atlantic Deep Water* (*NADW*)*:* At a reduced number of deep stations (depth > 1500 m) in the southwest part of the surveyed region, NADW, which is characterised by its depth-decreasing thermohaline properties (Ambar et al., 2002), has been found. The study of this water does not fall within the scope of this work.

3.2. Geostrophic calculations

There are different choices of a reference level to carry out geostrophic calculations in the Gulf of Cadiz in the literature: García et al. (2002) estimate the surface currents with reference to both 100 and 200 m. Ambar et al. (2002) adopt 2000 m as the no-motion surface. Ochoa and Bray (1991) postulated the interface between MW and NACW as the no-motion surface, and Sánchez and Relvas (2003) take 400 m as the reference surface.

An adequate reference level, which would be an (intuitively) motionless surface, should be the interface separating NACW from MW, at least in the vicinity of the Strait of Gibraltar, where MW is found at shallower depths. Since the flows have opposite directions, in this hypothetical interface the velocity will be near zero. Such a particular reference level has to maximise the inflow to the Strait of Gibraltar and the condition of maximisation determines, in turn, the depth of the "best" reference level. In addition, this level would gather conditions to be considered a motionless surface.

To this aim, the geostrophic volume transport towards the Strait of Gibraltar has been computed for different choices of the reference level. Details of this procedure can be found in Criado-Aldeanueva (2004). The isolines of geostrophic transport are then plotted starting from the zero value, which has been selected as the closest-to-shore isoline that crosses the full domain from west to east. Fig. 3(A) shows one of the geostrophic maps produced (the one with the reference in $Z_{\mathrm{ref}} = 300\,m$). From plots like this, the transport towards the Strait is easily computed. The maximum is reached when the reference level is around 300 m (between 300 and 325, see Fig. 3(B)). For this depth, the estimated transport to the Strait is 0.8 Sv (Fig. 3(B)), in good

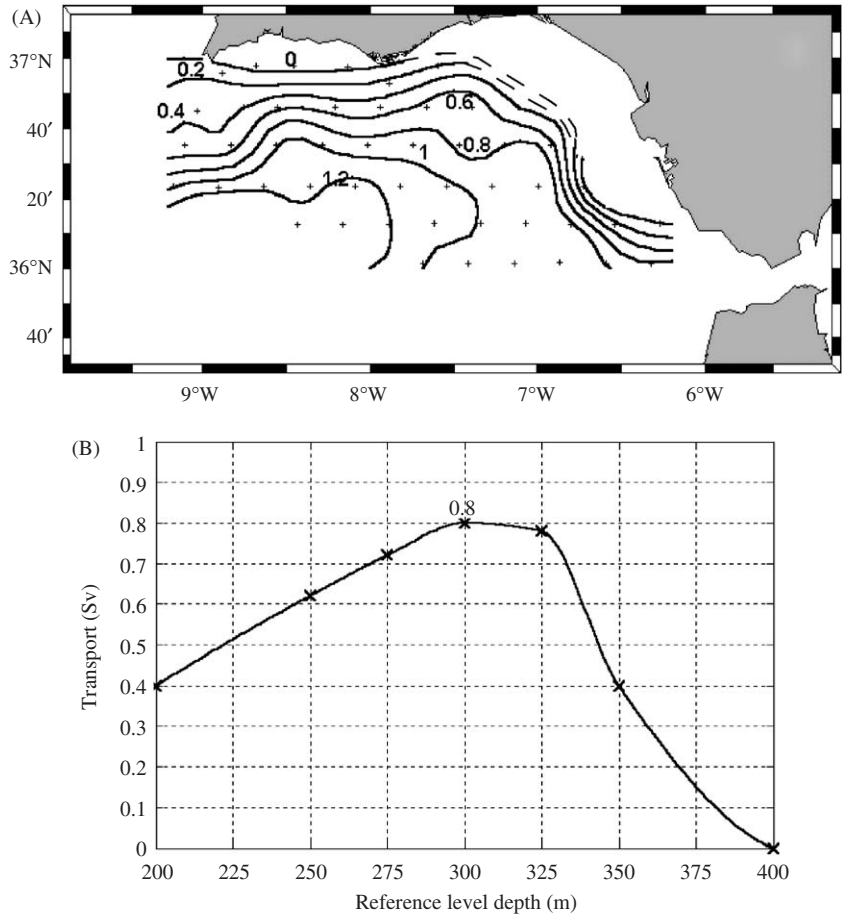

Fig. 3. (A) Isolines of geostrophic volume transport (Sv) during Macroscale using $Z = 300$ m as reference level. Notice that the lines follow two paths: one feeds the inflow to the Strait of Gibraltar and another recirculates towards the Atlantic. (B) Estimation of geostrophic volume transport (Sv) towards the Strait of Gibraltar as a function of the reference level depth (m) from Macroscale data. The maximum is reached at about 300 m.

agreement with the values of Bryden et al. (1994) and Baringer and Price (1997). The imposition of this additional condition on geostrophic transport is, to a certain extent, a technique comparable with inverse methods (Tarantolla, 1987; Bennett, 1992; Bennett and Chua, 1992; Parker, 1994). Nevertheless, the technique has some weak points, which must be discussed:

The inflow through the Strait of Gibraltar has important subinertial fluctuations, and there is no precise value that can be used as a reference to check our computations. In other words, it is not possible to affirm that 0.8 Sv, for instance, is the best value. However, using a maximisation condition instead of a concrete value avoids throwing uncertainty on the Z_{ref} value. The fact that geostrophic transport computations reproduce reasonably well the magnitude of the mean inflow to the Mediterranean supports the choice of the reference surface.

The section through which transport is computed does not completely cover the north–south section of the Strait of Gibraltar (Fig. 3(A)). But, from a certain isoline (about 0.8 Sv for $Z_{\text{ref}} = 300\,m$, see Fig. 3(A) again), the trajectory curves clearly to the south, suggesting that flow recirculation towards the Strait is quite improbable. More likely, water recirculates towards the Atlantic either to feed the anticyclonic gyre suggested in Fig. 3(A) or to form an eastern boundary current that will merge downstream with the Canary Current.

It can be argued that the criterion used to situate the zero transport isoline ignores possible inputs to the transport from the region to the north of it;

that is, water coming from the continental shelf (Fig. 3(A)). However, this choice is the only one with physical meaning, since the geostrophic function cannot intersect the coast. Moreover, the circulation on the continental shelf consists in a cyclonic cell in the eastern part (García Lafuente et al., 2006), so that the ignored transport, if any, cannot be too considerable.

Another objection arises as to whether the value of Z_{ref} obtained in the vicinity of the Strait of Gibraltar is adequate for the rest of the basin. It is well-known that MW sinks as it moves westwards (Zenk, 1970; Ambar and Howe, 1979a, b; Ambar et al., 2002), and thus the estimated reference surface will not coincide with a "interface" through all the basin. However, in the central region of the Gulf, where MW has sunk considerably, its influence on the motion of the shallower reference layer should not be that notable and the identification of the reference level with an almost motionless surface would still remain valid.

The possibility of using ADCP data to reference geostrophic computations has been considered. With the configuration adopted in the ADCP sampling, the rms error of ADCP velocities is $\geqslant 6\,\mathrm{cm\,s^{-1}}$, which is greater than the background velocity in the interior, i.e. velocity in the range 200–400 m. Therefore, these data do not help to select the reference level. However, geostrophic velocity shear (thermal wind) has been satisfactorily compared with ADCP vertical profiles.

3.3. Large-scale patterns: hydrological features and general circulation

The surface of the central Gulf of Cadiz is occupied (Figs. 4(A–C)) by a core of SAW with γ_t about $26.2\,\mathrm{kg\,m^{-3}}$. This core, as will be shown below, constitutes the limit of an anticyclonic meander referred in the literature and detected in previous surveys carried out in the area (Rubín et al., 1997, 1999; Prieto et al., 1999). In this central region, the geostrophic velocities are rather slow (Fig. 4(D)).

At intermediate depths, the Gulf of Cadiz is occupied mostly by NACW that upwells in the continental shelf, preferably in two well differentiated areas that coincide with Cape St. Vincent and Cape St. Maria, the two most important capes on the southwest coast of the Iberian Peninsula. The upwellings are identified by lower temperature and salinity waters and are dominant features in spring–summer, the upwelling season (Fiúza 1983; Folkard et al., 1997; Relvas and Barton, 2002; Sánchez and Relvas, 2003).

The upwelling off Cape St. Vincent appears to belong to the almost permanent upwelling system off western Portugal during the spring and summer months, when northerlies, related to the location of the Azores High, produce upwelling due to Ekman transport in the surface layer (Fiúza et al., 1982). However, the upwelling south of Cape St. Vincent takes place in an area that does not gather the

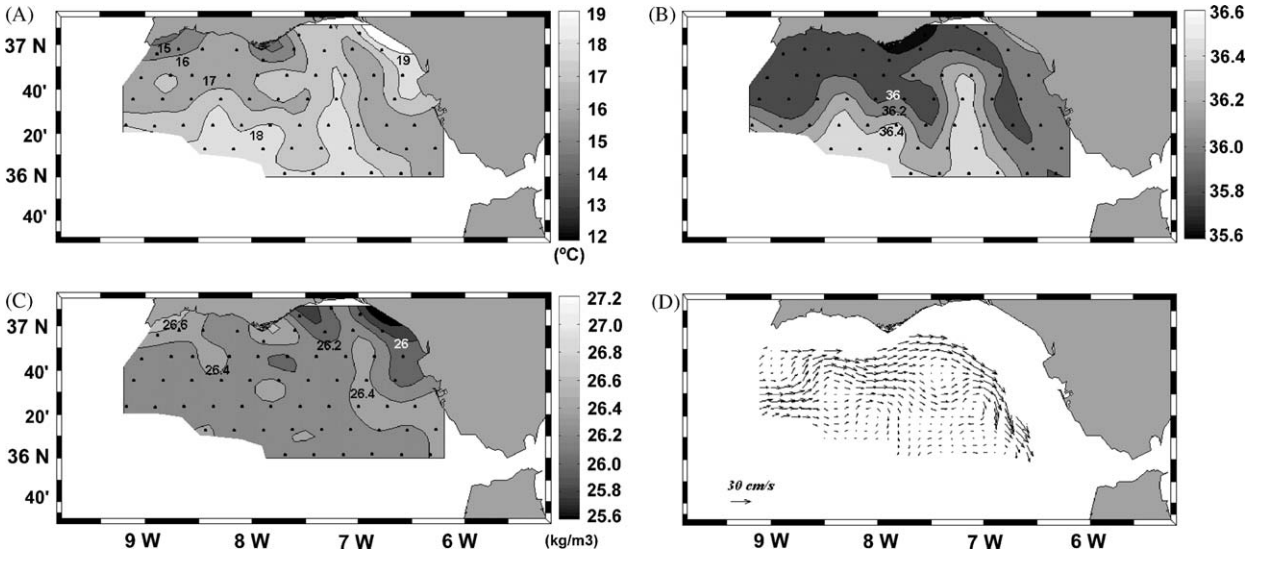

Fig. 4. Temperature (°C, panel A), salinity (panel B), density (γ_t, $\mathrm{kg\,m^{-3}}$, panel C) and geostrophic velocity at 10 m depth referred to 300 m (panel D) from Macroscale data. Stations have been marked in panels (A–C).

necessary conditions for coastal upwelling, as it is further south of the influence of the Portuguese coast. It could be related to Ekman pumping in the surface Ekman layer, an open-sea process linked to a positive wind curl over the area (Sánchez and Relvas, 2003). The positive vertical component of wind curl produces ascending velocities at the base of the surface Ekman layer that produce uprising of the isopycnes and advect dense water from the ocean's interior close to the surface. This upwelling induces cyclonic circulation to compensate the baroclinic pressure field. The Ekman theory should not be considered as instantaneous but rather in the sense that in a region where the vertical component of the wind curl is positive on average, the ocean will exhibit a cyclonic circulation and upwelling-favourable conditions. Fig. 5, which shows the monthly (May) average of the vertical component of the wind curl computed from scatterometer data, indicates that the region off west Portugal, and particularly the area south of Cape St. Vincent, has positive wind curl, supporting the hypothesis of upwelling related to Ekman pumping. Obviously, this upwelling is enhanced under favourable wind conditions, that is, westerlies, which produce additional coastal upwelling.

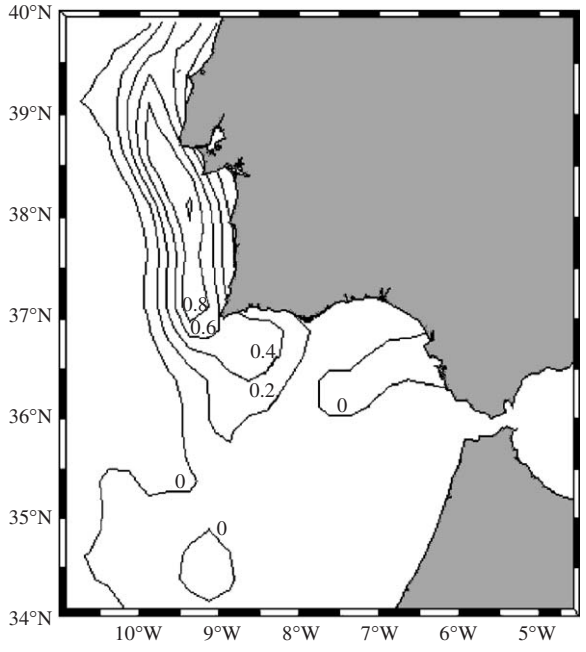

Fig. 5. Monthly (May) average of the vertical component of the wind curl ($\times 10^{-4}\,s^{-1}$) computed from scatterometer data. Positive values are found in the western and southwestern Iberia.

Upwelling off Cape St. Maria seems to be an exclusively coastal process that closely follows the change in the local wind regime. Under westerlies, upwelled waters off Cape St. Vincent are advected to the east by the main current, reaching the vicinity of Cape St. Maria, where they join the waters upwelled there (Fig. 6(A)). If the wind is favourable, waters keep on moving from Cape St. Maria eastwards constituting, in appearance, the Huelva Front (see Fig. 6(A) again). In contrast, under easterlies (Fig. 6(B)), the upwelling off Cape St. Maria disappears, and apparently this is also the case with the Huelva Front, at least as regards its surface thermal signature (García Lafuente et al., 2006).

Geostrophic velocities at 10 m referred to 300 m (Fig. 4(D)) show a general circulation pattern from west to east with some meanders and a bifurcation around 8 °W in two branches that join together downstream at 7 °W, and describe an anticyclonic meander with moderate velocities (~30 cm s^{-1}). The

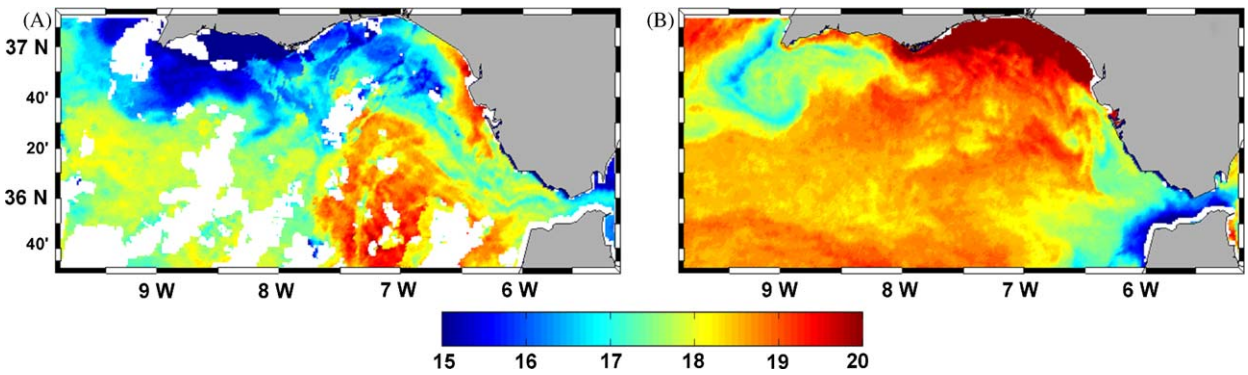

Fig. 6. Sea surface temperature (SST) satellite images (°C) for 13 May, the day previous to Mesoscale 1 sampling (panel A) and for 29 May, during Mesoscale 2 (panel B). Westerlies were dominant in the first mesoscale and easterlies in the second one (see also Fig. 11), thus promoting great variability of the surface thermal patterns.

overall circulation pattern is in good agreement with the climatological results obtained by Sánchez and Relvas (2003). The surface salinity distribution shows saltier waters in the central part, whereas the water in the northern area is less saline. The main feature is the presence of two filaments of low salinity, which stretch to the south from Cape St. Maria and parallel to the coast of Huelva and Cadiz (Fig. 4(B)) (see Section 3.4). The density field shows a region of less dense water on the continental shelf, corresponding to the warm water present in that area, and two regions of denser water off Capes St. Vincent and St. Maria, that corresponds with the upwelled water.

Next to the Guadalquivir river mouth (Fig. 4(A)) is a region of warm shelf water, which stretches to around 7 °W and undergoes noticeable wind-induced variability. Separating the warm shelf waters and the central warm core is a tongue of colder water stretching NW–SE, which has been traditionally denoted as the Huelva Front (Stevenson, 1977; Fiúza, 1983), which is enhanced under westerlies (Relvas and Barton, 2002).

The main characteristic of the fields at 50 m (Fig. 7) is the gradient of the isolines from the coast outwards, NACW (colder and fresher) being found nearest to the coast and SAW (warmer and more saline) in the central region of the Gulf. A region of NACW off Cape St. Maria is more visible in the salinity field, which divides into two parts the central SAW core. Compared with the surface description, the signature of warm water on the Spanish coastal shelf has disappeared at this depth and NACW detected off Capes St. Vincent and St. Maria now stretches along the entire continental shelf and slope. The density field (panel c of Fig. 7) is dominated by the temperature as shown by the presence of denser NACW in the shelf (where waters are colder) and lighter SAW in the central region (where waters are warmer). The geostrophic velocities at 50 m maintain the same circulation pattern than on the surface, with slightly lower values (around 20–25 cm s^{-1} in the northern region, where the current is strongest). The outstanding characteristics of the variables at 100 m (not shown) are the visible presence of the central warm core of SAW, the still noticeable signal in salinity of the filament off Cape St. Maria, and the anticyclonic circulation parallel to the coast with lower velocities than in shallower depths.

3.4. Mesoscale circulation: the filament of Cape St. Maria

The filament of Cape St. Maria refers to the filament of colder and fresher water that stretches south from about Cape St. Maria along the 7.5 °W meridian (Fig. 4(B)). The filament leaves a distinguishable footprint in the T/S vertical profiles and, particularly, in the TS diagram (Fig. 8(A)): around $S = 36.0$ and between 15.0 and 16.0 °C, a peak that breaks the linear relation characteristic of NACW is

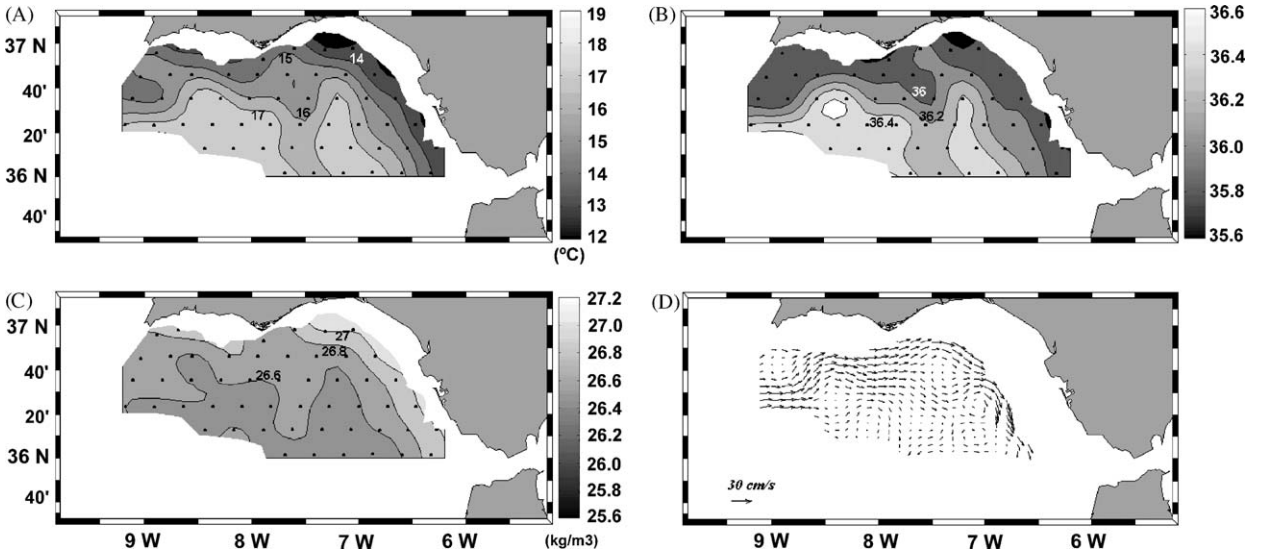

Fig. 7. Temperature (°C, panel A), salinity (panel B), density (γ_t, kg m^{-3}, panel C) and geostrophic velocity referred to 300 m (panel D) at 50 m depth from Macroscale data. Stations deeper than 50 m have been marked in panels (A–C).

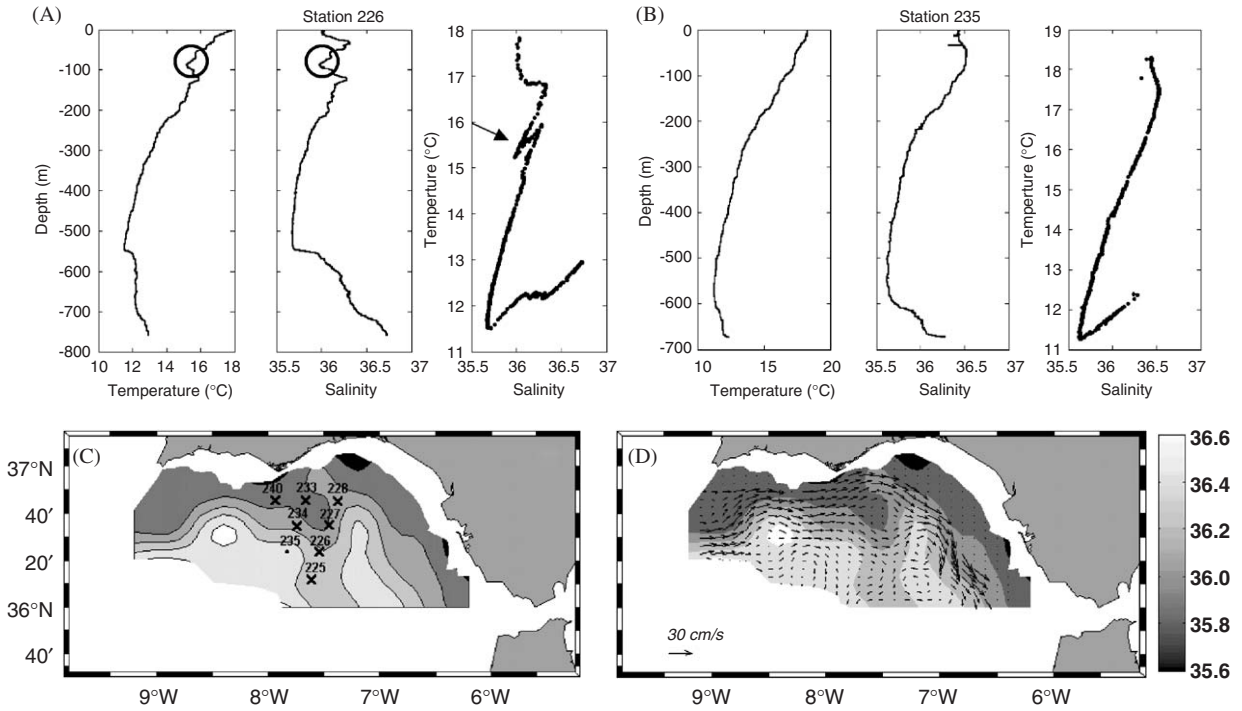

Fig. 8. (A) Temperature and salinity profiles and *TS* diagram of station 226 of Macroscale (see panel C for location) inside Cape St. Maria filament. The peak marked around $S = 36.0$ and between 15.0 and 16.0 °C in the *TS* diagram corresponds to the intrusion of colder and fresher waters in the upper 100 m of the water column (circled). All the stations inside the filament (see panel C) exhibit similar characteristics. (B) The same as in panel (A) for station 235 outside the filament. No anomalous behaviour is detected in the linear *TS* relation of NACW. (C) Stations inside the filament (crosses) superposed to the salinity field at 50 m depth during Macroscale. Station 235, outside the filament, is also marked with a point. (D) Geostrophic velocity at 50 m depth referred to 300 m superposed to the salinity field at 50 m.

clearly detected. The peak indicates the presence of colder and fresher waters in the first 100 m of the water column. All the stations that share this specific feature are marked by crosses in Fig. 8(C), and the resulting spatial pattern matches the low-salinity tongue of Figs. 4(B) and 7(B) quite accurately. In contrast, stations outside the filament maintain the linear *T*–*S* relation of the NACW (Fig. 8(B)).

The hypothesis is that the source of the filament are waters upwelled off Cape St. Vincent and advected to the east by the main current. This current follows the salinity isolines in the western part of the domain (Fig. 8(D)) and bifurcates around 7.5 °W. The southern branch would carry the upwelled water in a north–south direction, giving rise to the filament off Cape St. Maria.

Some further insight on the nature of the filament is provided by an EOF analysis. Fig. 9 shows the results of such analysis restricted to the depth range of 20–160 m. This range has been chosen because the filament is very clear at 50 m (Fig. 8(C)) but not so clear at 100 m (not shown), for which it is hoped that this depth interval captures first the emergent features of the filament and then their subsequent fading out with depth. Fig. 9(A) is the spatial map of the first mode of the temperature and salinity anomalies (the spatial mean given in Eq. (2) has been removed in the EOF analysis), and Fig. 9(B) shows the amplitude coefficients of these modes for all depths. The variance explained by the first mode is high for the two variables (62.5% for temperature and about 67% for salinity) and the spatial patterns reveal clearly the presence of the filament. The stations marked with a cross in Fig. 8(C) also have been plotted in Fig. 9(A), and all of them fall within the feature revealed by the first mode, both in temperature and salinity.

The first mode predicts colder and fresher waters for the filament, in good agreement with its hydrological description. The lower salinity follows from the fact that the spatial map shows negative

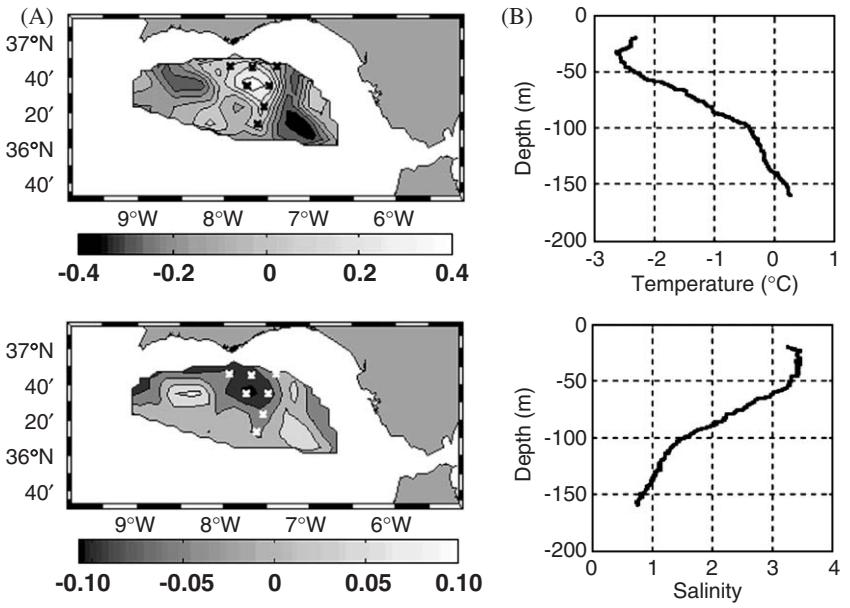

Fig. 9. (A) Spatial map of the first mode of temperature (upper panel) and salinity (lower panel) anomalies of the EOF analysis performed in the range 20–160 m from Macroscale data. Stations inside the filament have been marked with X (see Fig. 7C). The first mode reveals the presence of the filament both in temperature and salinity. (B) Amplitude coefficients of the first mode of temperature (upper panel) and salinity (lower panel) of the EOF analysis. The maximum (absolute) value is reached at about 40–50 m, where the filament is more pronounced.

anomaly and the amplitude coefficients are positive. In contrast, the temperature anomaly is positive, but the amplitude coefficients are negative until 150 m, where they change sign. The EOF analysis clearly suggests that the filament is more pronounced between 40 and 50 m, since the amplitude coefficients reach their maximum absolute value, after which its signature progressively vanishes (the coefficients decrease in absolute value) until it disappears around 150 m in temperature and, several metres below, in salinity. Lastly, the high variance captured by the first mode indicates that the filament is likely the most relevant feature in this depth range.

3.5. Distribution and circulation of NACW

NACW is the most important water mass in at least the first 1000 m of the water column in the central part of the Gulf of Cadiz. Fig. 2 shows that the surface $\gamma_t = 27.0\,\mathrm{kg\,m^{-3}}$ corresponds to NACW that has suffered very little mixing both with upper warm surface water and with lower MW. As a result, *TS* properties on the surface $\gamma_t = 27.0\,\mathrm{kg\,m^{-3}}$ are practically constant ($T \approx 13.2\,^{\circ}\mathrm{C}$, $S \approx 35.8$). Water with $\gamma_t < 27.0\,\mathrm{kg\,m^{-3}}$ may be sensitive to surface heating making its *TS* signature diverge from the line of NACW, moving vertically along the temperature axis in the *TS* diagram (Fig. 2). For $\gamma_t > 27.0\,\mathrm{kg\,m^{-3}}$, in some stations the water is prone to feel the effect of MW in such a way that the divergence from the line of NACW is along the salinity axis towards more saline values (Fig. 2). When the Gulf of Cadiz is taken into consideration as a whole, $\gamma_t = 27.0\,\mathrm{kg\,m^{-3}}$ represents, in spatial average, the purest NACW. The depth of the surface $\gamma_t = 27.0\,\mathrm{kg\,m^{-3}}$ (Fig. 10(A), contours) is greater for stations furthest away from the coast, and the depth gradient is fairly significant in the easternmost region of the Gulf, due to the interaction in this area of NACW with MW leaving the Strait of Gibraltar. In the central part of the Gulf, far from the direct influence of MW, the surface $\gamma_t = 27.0\,\mathrm{kg\,m^{-3}}$ is located at a depth of about 250–300 m.

Besides this homogeneity, things are notably more varied when we consider the surfaces $\gamma_t = 26.6$ and $27.3\,\mathrm{kg\,m^{-3}}$, regarded as the limits of NACW (Fig. 10(B, D)). $\gamma_t = 26.6\,\mathrm{kg\,m^{-3}}$ is located at depths above 70 m and the distribution of the salinity on this surface shows saltier water to the south and fresher water to the north. The circulation at this surface is similar to the one at 50 m (Fig. 7(D)). It is predominantly anticyclonic and the

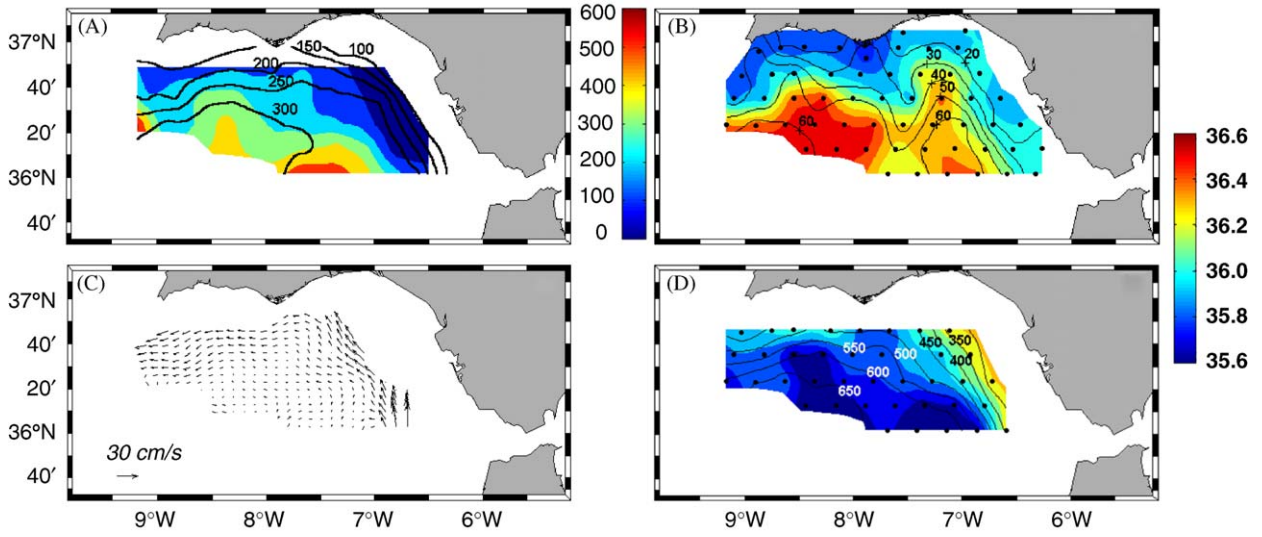

Fig. 10. (A) Depth (metres, in contours) of $\gamma_t = 27.0\,\mathrm{kg\,m^{-3}}$ and thickness (metres, in colour scale) of the NACW layer with $S<35.8$ from Macroscale sampling. (B) Salinity (colour scale) and depth (metres, in contours) of the $\gamma_t = 26.6\,\mathrm{kg\,m^{-3}}$ isopycne regarded as the upper limit of NACW. Stations involved in the computations have been marked. (C) Geostrophic velocity at $\gamma_t = 27.3\,\mathrm{kg\,m^{-3}}$ referred to 300 m. The geostrophic velocity field depicts the vein of MW that stretches westwards in the eastern and northern part of the Gulf. (D) The same as in panel (B) for the $\gamma_t = 27.3\,\mathrm{kg\,m^{-3}}$ isopycne, regarded as the lower limit of NACW.

velocities are moderate, particularly in the northern area of the domain with values around $30\,\mathrm{cm\,s^{-1}}$. This isopycne is of great interest in biological studies in the Gulf of Cadiz, as it can be considered a nutrient tracer and an indicator of the depth of the Deep Fluorescence Maximum (Navarro et al., 2006). In contrast, $\gamma_t = 27.3\,\mathrm{kg\,m^{-3}}$ corresponds to deeper water (below 300–400 m) and the distribution of salinity on this surface now shows less-saline waters to the south and traces of salty MW at the eastern stations. The circulation at this depth reflects the vein of MW stretching from east to west in the eastern and northern part of the Gulf of Cadiz (Fig. 10(C)).

The thickness of NACW could be estimated as the difference between the depth of the surfaces $\gamma_t = 26.6$ and $27.3\,\mathrm{kg\,m^{-3}}$, its theoretical limits. But it is probably more convenient to combine the properties of surface $\gamma_t = 27.0\,\mathrm{kg\,m^{-3}}$ with that of minimum salinity to obtain the thickness of NACW with $S<35.8$, regarded as the purest NACW. The salinity minimum is on average about 35.7 and thus, due to the shape of the *TS* diagram, the value of $S = 35.8$ is reached at two different depths, the upper one coinciding with the depth of $\gamma_t = 27.0\,\mathrm{kg\,m^{-3}}$ (see Fig. 2). These two depths can be considered acceptable as the upper and lower boundaries of purest NACW. In the central region of the Gulf, the thickness of this layer reaches 400 or 500 m, whereas at the stations nearest to the coast it is only 100 or 200 m (Fig. 10(A)).

3.6. Variability of currents and geostrophic transports

The wind regime during the three legs of GOLFO 2001 survey varied significantly (Fig. 11). Mesoscale 1 and Macroscale were (mainly) accomplished under westerlies, whereas Mesoscale 2 was sampled under easterlies. Wind changes induced noticeable variability in hydrological, chemical and dynamical patterns, whose detailed description is out of the scope of this work. However, it is worth to outline some of the wind-induced changes in the circulation of the Gulf of Cadiz. Although the general circulation keeps the same characteristic pattern, some significant differences can be detected (see Fig. 12): in Mesoscale 1, the velocity in the vicinity of Cape St. Maria at 10 m depth is intense (the rms velocity is $20\,\mathrm{cm\,s^{-1}}$) and anticyclonic (Fig. 12(A)). This behaviour has been altered in Mesoscale 2, where the current is more sinuous, although the energy, indicated by the rms velocity, is similar for the same depth. In its route, it traces first a cyclonic meander off the cape (~8 °W) and then recuperates the anticyclonic movement in a new meander more

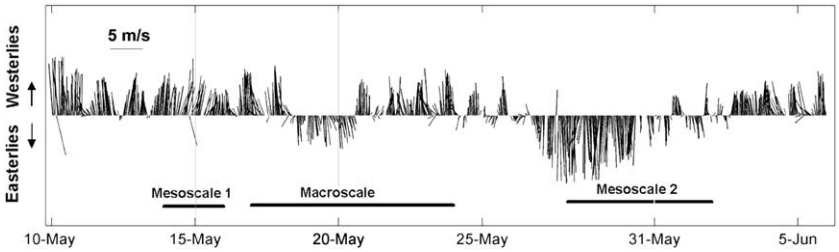

Fig. 11. Stick diagram of the wind regime from the RAP buoy (see Fig. 1 for location) during May–June 2001. Time period of each survey has been indicated. Westerlies prevailed during Mesoscale 1 and the previous days; Macroscale was sampled under both regimes although westerlies were more frequent and intense. Mesoscale 2 was influenced by the moderate to strong and rather persistent episode of easterlies.

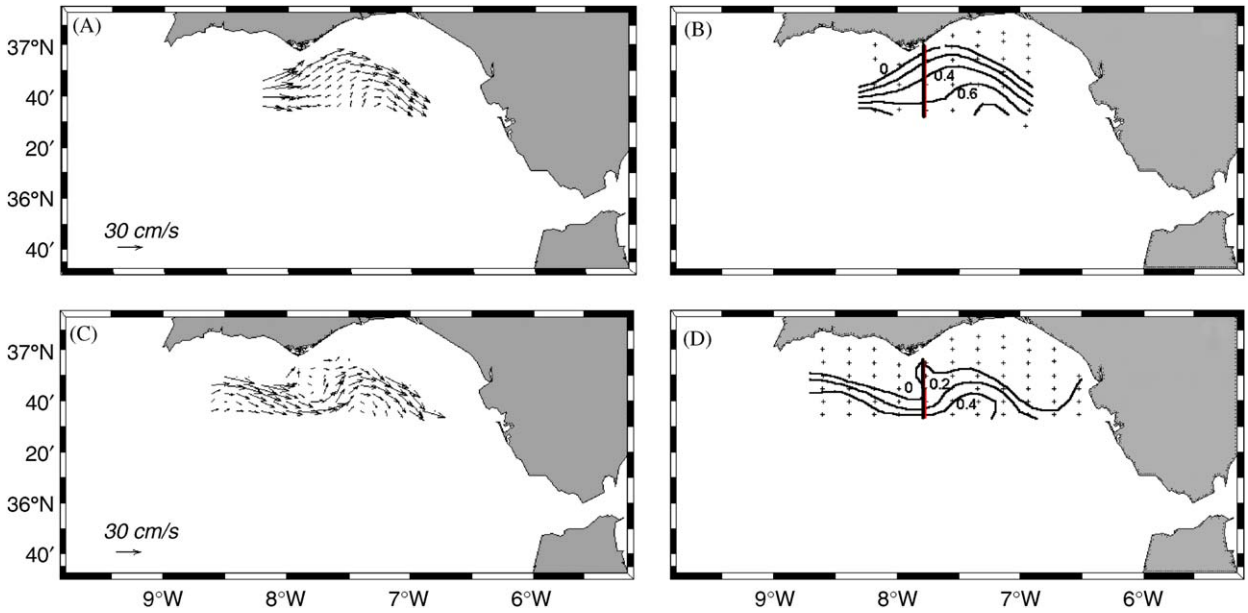

Fig. 12. Geostrophic velocity at 10 m depth referred to 300 m for Mesoscale 1 (panel A) and Mesoscale 2 (panel C) and geostrophic transport (Sv) in the upper 300 m for Mesoscale 1 (panel B) and Mesoscale 2 (panel D). Stations are marked in panels (B and D). The solid line in panels (B and D) represents the section in front of Cape St. Maria used to compare geostrophic transports.

to the east at ~7.25 °W (Fig. 12(C)). An explanation for this variability is that, in Mesoscale 1, westerlies, that favours upwelling, retain the coastal countercurrent moving westwards through the northern part of the Gulf (Fiúza, 1983; Folkard et al., 1997; Relvas and Barton, 2002; Sánchez and Relvas, 2003; García-Lafuente et al., 2006), for which reason the main current has nothing opposing its movement eastwards. In Mesoscale 2, under easterlies, the upwelling weakens, allowing the coastal countercurrent to progress towards Cape St. Maria and farther west, thereby forcing the main current away from the cape and to form the characteristic feature of a double meander.

The geostrophic transports exhibit more variability. In Mesoscale 1, the transport isolines are convex and approach Cape St. Maria (Fig. 12(B)), whereas in Mesoscale 2 they remain faraway from the cape and have, similarly to what happened with the currents, a double meander feature (Fig. 12(D)). The volume transports also differ: in Mesoscale 1, 0.78 Sv flowed through the section marked in Fig. 12(B,D) while in Mesoscale 2, it flowed only 0.51. During the Macroscale (Fig. 3(A)), the flow was 0.69 Sv, a volume transport midway between Mesoscales 1 and 2. This variability obviously follows the wind variations and is in good agreement with the literature on exchanges through the Strait of Gibraltar, which predicts an increase of inflow to the Mediterranean under westerlies and a decrease under easterlies. (García-Lafuente et al., 2002a, b).

4. Summary

From the data collected during GOLFO 2001 survey, a study has been conducted on the circulation and distribution of water masses in the Gulf of Cadiz in the spring of 2001, and on its meteorologically forced variability. Most of the experimental information used to conduct the study consisted of CTD data, with which the geostrophic analysis in the outer region of the Gulf of Cadiz was carried out. The meteorological conditions, studied from the registers of the station of Hespérides and the RAP buoy, as well as the scatterometer data, show that, in Mesoscale 1 and the greater part of the Macroscale, westerlies were dominant. In Mesoscale 2, there was a period of strong easterlies. This variability has made it possible to study the response of the oceanographic features to meteorological forcing using in situ data.

NACW ($\gamma_t = 26.6-27.3\,\mathrm{kg\,m^{-3}}$) is a very representative water mass in the first 1000 m of the water column. In $\gamma_t = 27.0\,\mathrm{kg\,m^{-3}}$, the temperature and salinity are practically uniform. To the north of the domain, the lower layer of NACW ($\gamma_t = 27.3\,\mathrm{kg\,m^{-3}}$) is entrained by MW towards the open ocean and the upper layer of NACW ($\gamma_t = 26.6\,\mathrm{kg\,m^{-3}}$) already forms part of the anticyclonic surface circulation of the Gulf of Cadiz. In the central region, main reservoir of NACW, the movement is very limited. SAW ($T > 16.0\,^{\circ}\mathrm{C}$, $S \approx 36.4$ and $\gamma_t \leqslant 26.7\,\mathrm{kg\,m^{-3}}$) is found between the surface and 100 m and has its origin in shallow NACW that has been modified by air–sea interactions. Two main maxima were detected in the *TS* diagram corresponding to the two cores (upper and lower) of MW with different densities, respectively, $\gamma_t \approx 27.5$ and $27.8\,\mathrm{kg\,m^{-3}}$ centred near 800 and 1200 m.

NACW mainly upwells in the vicinity of Capes St. Vincent and St. Maria. The upwelling off Cape St. Vincent seems to be related to Ekman pumping in the surface Ekman layer, an open-sea process linked to a positive wind curl over the area that produces uprising of the isopycnes and advects dense water from the ocean's interior close to the surface. The upwelling off Cape St. Maria is a more likely coastal process with a short time response to changes in the wind regime: it is enhanced under westerlies, and it weakens, and even fades out, under easterlies. The waters upwelled off Cape St. Vincent move eastwards following the main current until reaching $\sim 7.5\,^{\circ}\mathrm{W}$, where they form the filament of Cape St. Maria, which reaches its maximum signature at about 40–50 m.

The general surface circulation in the Gulf of Cadiz is anticyclonic with short-term variations. Under westerlies, the geostrophic current, referred to 300 m so as to maximise the inflow to the Strait of Gibraltar, approaches Cape St. Maria more than under easterlies, possibly because, in this last case, the coastal countercurrent forces it away from the cape. The geostrophic transport in any north–south section is 30% greater under westerlies than under easterlies.

In the Macroscale samplings, with a greater geographical scope, it is important to note that the current bifurcates into two branches at $7.5\,^{\circ}\mathrm{W}$ (off Cape St. Maria), which then join together downstream. Once united, the current follows two paths on approaching the Strait of Gibraltar: one of income to the Mediterranean Sea through the Strait and another turning south and forming a meander that joins the Canary Current.

Acknowledgements

We thank the UIB-IMEDEA (Special Action CICYT, REN2000-2599-E) for the dissemination of the software used for the optimal interpolation. Wind data from the RAP buoy have been kindly provided by Puertos del Estado. Wind processing of the scatterometer data has been courtesy of the Servicio de Teledetección de Color Oceánico of the ICMAN-CSIC. We are also indebted to the crew of BIO Hespérides for his work during GOLFO 2001 survey. F. Criado Aldeanueva is much obliged to the Spanish Ministry of Education and Science for awarding him a F.P.U. grant (reference No. AP2000-3951).

References

Álvarez, A., López, C., Riera, M., Hernández-García, E., Tintoré, J., 2000. Forecasting the SST space–time variability of the Alborán Sea with generic algorithms. Geophysical Research Letters 27 (17), 2709–2712.

Alves, M., Gaillard, F., Sparrow, M., Knoll, M., Giraud, S., 2002. Circulation patterns and transport of the Azores Front-Current System. Issue Series Title: Deep-Sea Research II 49, 3983–4002.

Ambar, I., Howe, M.R., 1979a. Observations of the Mediterranean outflow I: mixing in the Mediterranean outflow. Deep-Sea Research 26A, 535–554.

Ambar, I., Howe, M.R., 1979b. Observations of the Mediterranean outflow II: the deep circulation in the vicinity of the Gulf of Cadiz. Deep-Sea Research 26A, 555–568.

Ambar, I., Serra, N., Brogueira, M.J., Cabeçadas, G., Abrantes, F., Freitas, P., Gonçalves, C., Gonzalez, N., 2002. Physical, chemical and sedimentological aspects of the Mediterranean outflow off Iberia. Deep-Sea Research II 49, 4163–4177.

Baringer, M.O., Price, J.F., 1997. Mixing and spreading of the Mediterranean outflow. Journal of Physical Oceanography 27 (8), 1654–1677.

Bennett, A.F., 1992. Inverse Methods in Physical Oceanography. Cambridge Monographs on Mechanics and Applied Mathematics. Cambridge University Press, Cambridge, (347pp).

Bennett, A.F., Chua, B.S., 1992. Open ocean modelling as an inverse problem: the primitive equations. Monthly Weather Review 112, 1326–1336.

Bryden, H.L., Candela, J., Kinder, T.H., 1994. Exchange through the Strait of Gibraltar. Progress in Oceanography 33, 201–248.

Criado-Aldeanueva, F., 2004. Distribución y Circulación de Masas de Agua en el Golfo de Cádiz. Variabilidad Inducida por el Forzamiento Meteorológico. Ph.D. Thesis, University of Málaga. ISBN: 84-689-0245-4. Published by the Publication Service University of Málaga (in Spanish).

Fiúza, A.F.G., 1983. Upwelling patterns off Portugal. In: Suess, E., Thiede, J. (Eds.), Coastal Upwelling. Plenum, New York, pp. 85–98.

Fiúza, A.F.G., de Macedo, M.E., Guerreiro, M.R., 1982. Climatological space and time variations of the Portuguese coastal upwelling. Oceanologica Acta 5, 31–40.

Folkard, A.M., Davies, P.A., Fiúza, A.F.G., Ambar, I., 1997. Remotely sensed sea surface thermal patterns in the Gulf of Cadiz and Strait of Gibraltar: variability, correlations and relationships with the surface wind field. Journal of Geophysical Research 102, 5669–5683.

Gandin, L., 1963. Objective Analysis of Meteorological Fields (Transl. from Russian by Israel Program for Scientific Translations), 1965 (NTIS No. TT65-50007).

García, C.M., Prieto, L., Vargas, M., Echevarría, F., García Lafuente, J., Ruiz, J., Rubín, P., 2002. Hydrodynamics and the spatial distribution of Plankton and TEP in the Gulf of Cádiz (SW Iberian Peninsula). Journal of Plankton Research 24 (8), 817–833.

García-Lafuente, J., Álvarez Fanjul, E., Vargas, J.M., Ratsimandresy, A., 2002a. Subinertial variability in the flow through the Strait of Gibraltar. Journal of Geophysical Research 107, c10, doi:10.1029/2001JC00104.

García Lafuente, J., Delgado, J., Vargas, J.M., Vargas, M., Plaza, F., Sarhan, T., 2002b. Low-frequency variability of the exchanged flows through the Strait of Gibraltar during CANIGO. Deep-Sea Research II 49, 4051–4067.

García Lafuente, J., Delgado, J., Criado-Aldeanueva, F., Bruno, M., Del Río, J., Vargas, J.M., 2006. Water mass circulation on the Continental Shelf of the Gulf of Cadiz. Deep-Sea Research II, this issue [doi:10.1016/j.dsr2.2006.04.011].

Gomis, D., Ruiz, S., Pedder, M.A., 2001. Diagnostic analysis of the 3D ageostrophic circulation from a multivariate analysis of CTD and ADCP Data. Deep-Sea Research I 48(1), 269–295.

Hernández-Guerra, A., Nykjaer, L., 1997. Sea surface variability off North-west Africa: 1981–1989. International Journal of Remote Sensing 18, 2539–2558.

Knoll, M., Lenz, B., Müller, T.J., Reppin, J., Siedler, G., 1999. Eastern Canary Basin Hidrography. Part I: Physical observations. Poster presented in CANIGO Final Conference, Las Palmas de Gran Canaria.

Lorenz, E.N., 1956. Empirical orthogonal functions and statistical weather prediction. Scientific Report No. 1, Statistical Forecasting Project. Department of Meteorology. MIT, Cambridge, MA, (49pp).

Madelain, F., 1970. Influence de la Topographie du Fond Sur L'ècoulement Mediterraneén entre le Détroit de Gibraltar et le Cap Saint -Vincent. Cahiers Océanographiques 22, 43–61 (in French).

Navarro, G., Ruiz, J., García, C.M., Criado-Aldeanueva, F., Echevarría, F., 2006. Basin Scale Structures Governing the Position of the Deep Fluorescence Maximum in the Gulf of Cadiz. Deep-Sea Research II, this issue [doi:10.1016/j.dsr2.2006.04.013].

Obukhov, A.M., 1947. Statistically homogeneous fields on a sphere. Uspekhi Matematicheskikh Nauk 2, 196–198.

Ochoa, J., Bray, N.A., 1991. Water masses exchange in the Gulf of Cadiz. Deep-Sea Research 38 (Suppl. 1), S465–S503.

Parada, M., Cantón, M., 1998. Sea surface temperature variability in Alboran Sea from satellite data. International Journal of Remote Sensing 19, 2439–2450.

Parker, R.L., 1994. Geophysical Inverse Theory. Princeton University Press, Princeton, NJ.

Prieto, L., García, C.M., Corzo, A., Ruiz Segura, J., Echevarría, F., 1999. Phytoplankton, bacterioplankton and nitrate reductase activity distribution in relation to physical structure in the Northern Alboran Sea and Gulf of Cadiz (Southern Iberian Peninsula). Boletin del Instituto Espanol de Oceanografia 15, 401–411.

Relvas, P., Barton, E.D., 2002. Mesoscale patterns in the Cape Sao Vicente (Iberian Peninsula) upwelling region. Journal of Geophysical Research 107 (C10), 3164–3186.

Rubín, J.P., Cano, N., Arrate, P., García Lafuente, J., Escánez, J., Vargas, M., Alonso Santos, J.C., Hernández, F., 1997. El Ictioplancton, el Mesozooplancton y la Hidrología en el Golfo de Cádiz, Estrecho de Gibraltar y Sector Noroeste del Mar de Alborán en Julio de 1994. Informe Técnico del Instituto Español de Oceanografía 167, 44 (in Spanish).

Rubín, J.P., Cano, N., Prieto, L., García, C.M., Ruiz, J., Echevarría, F., Corzo, A., Gálvez, J.A., Lozano, F., Alonso Santos, J.C., Escánez, J., Juarez, A., Zabala, L., Hernández, F., García Lafuente, J., Vargas, M., 1999. La Estructura del Ecosistema Pelágico en Relación con las Condiciones Oceanográficas y Topográficas en el Golfo de Cádiz, Estrecho de Gibraltar y Mar de Alborán (Sector Noroeste) en Julio de 1995. Informe Técnico del Instituto Español de Oceanografía 175, 73 (in Spanish).

Ruiz Valero, S., 2000. Análisis Espacial Objetivo de Datos Oceanográficos: Aplicaciones en el Mar de Alborán. Ph.D. Thesis, University of Islas Baleares-IMEDEA (in Spanish).

Sánchez, R., Relvas, P., 2003. Spring—summer climatological circulation in the upper layer in the region of Cape St. Vincent, Southwest Portugal. ICES Journal of Marine Science 60, 1232–1250.

Stevenson, R.E., 1977. Huelva front and Malaga, Spain, Eddy chain as defined by satellite and oceanographic data. Deutsche Hydrographische Zeitschrift 30 (2), 51–53.

Tarantolla, A., 1987. Inverse Problem Theory. Methods for Data Fitting and Model Parameter Estimation. Elsevier Science Publishers, Amsterdam.

Thiébaux, H.J., Pedder, M.A., 1987. Spatial Objective Analysis with Applications in Atmospheric Sciences. Academic Press, New York, (299pp).

UNESCO, 1985. The International System of Units in Oceanography. UNESCO Technical Paper no. 45, Paris. United Nations Educational, Scientific and Cultural Organization.

Vargas, J.M., García-Lafuente, J., Delgado, J., Criado, F., 2003. Seasonal and wind-induced variability of sea surface temperature patterns in the Gulf of Cádiz. Journal of Marine Systems 38, 205–219.

Zenk, W., 1970. On the temperature and salinity structure of the Mediterranean water in the Northeast Atlantic. Deep-Sea Research 17, 627–631.